2

Advanced PFA thin porous membranes[1]

R. A. Minamisawa, R. L. Zimmerman, C. Muntele and D. ILA
Center for Irradiation Materials, Alabama A&M University
USA

1. Introduction

The invention of synthetic membranes in the middle of the last century was a significant development for industrial and research processes and "invaded" day-to-day life as an important technology for sustainable growth. Nowadays, nearly 50 years since the creation of synthetic polymer membranes, novel developments and refinements in membrane technology continue to be active themes of research; membrane technologies are now well accepted and cost-effective, conferring unique advantages over previous separation processes (Rogers *et al*., 1998).

Separation membranes are broadly applied in food, chemical and pharmaceutical industries. Particularly, filtration membranes have proven to be reliable devices for water filtration (Fologea, 2005; Henriquez, 2004; Li, 2001, 2003a; Mochel, 1984; Mutoh, 1987; Schenkel, 2003). However, advances in materials and membrane processing are still a key solution to purify water at lower costs and higher flux in societies where scarce water resource is a major issue (Wiesner & Chellam, 1999).

Porous membranes are thin sheets and hollow fibers generally formed from a continuous matrix structure containing a range of open pores or conduits of small size. Porous membranes having open pores, thereby imparting permeability, are classified in nanofiltration, ultrafiltration and microfiltration membranes, depending in the pore size (Vainrot *et al*., 2007).

Nanofiltration membranes have pores with diameter in the range of 3 nm and are used for treatment of slightly polluted water and for pretreatment in desalination processes. Commonly, an electrostatic charge is applied in the NF membrane in order to enhance salt rejection.

Ultrafiltration membranes and microfiltration membranes have, respectively, pore diameters in the range of 10-100 nm and up to 1 μm. Combined, these membranes are extensively used in wastewater treatment equipment for removing virus and bacteria, organic molecules and suspended matter. Separation capacity in these membranes is based on simple filtration, therefore, depending on the contaminant size in solution and on the diameter of the pores.

Ideally, porous membranes require high permeability, high selectivity, enhanced resistance to biofouling, and resistance against solvents, high- and low-pH environments, and

[1] U.S. Patent pending.

oxidizers. In other words, the material precursor for the membranes must be chemically resistant and the pores are required to have a homogeneous distribution in the pore size, fulfilling the high selectivity requirement, and a homogeneous spatial distribution of the pores, leading to enhanced mechanical resistance. Microbial fouling or biofouling has been the most complex challenge to eliminate (Girones *et al.*, 2005, Vainrot *et al.*, 2007). The solution for these problems lies in the development of innovative processes for fabrication of porous membranes as well as in the availability of new polymer precursors (Vainrot *et al.*, 2007).

Up to now, several materials and methods have been proposed to enhance properties in porous membranes, exploring from the polymer to the microelectronic technologies. However, currently there is no membrane available that fulfills all cost, quality and performance requirements, suggesting that the membrane technology is still in its early stage of development. The challenge lies in developing new fabrication methods able to process resistant materials into high flux porous membranes structures.

In this chapter a review is given of the main issues related to the fabrication of high performance porous thin film membranes and how this technology has been developed to keep the bottom-line of cost-benefit. We later introduce our recent results in the development of Perfluoroalkoxyethylene (PFA) fluorpolymer based thin porous membranes with enhanced separation capacity as well as being resistant to biofouling and harsh chemicals, using an ion beam nanofabrication technique. In addition, we describe the development of a feedback ion beam controlled system able to fabricate well shaped and well distributed micro and nanopores, and to monitor in real-time the pore formation.

2. Advances in porous membranes

Firstly, we briefly provide an overview in the current status and the advances in porous membrane fabrication. Membranes in separation modules are usually fluorpolymer based membranes due to their cost-effectiveness as well as their thermal stability and chemically inert properties, attributes that give excellent resistance to the devices. While these polymer properties are desirable for porous membranes, they also render the polymer unamenable to casting into well-shaped membranes by conventional processes. Because it is difficult to chemically etch this material, it is impractical to fabricate membranes with high pore quality regarding spatial and size distribution in fluorpolymer films; consequently, this type of membrane has low selectivity as well as low mechanical stability (Caplan *et al.*, 1997). Figure 1 displays an example of this type of tortuous path membrane.

Track-etched membranes (TEMs) are typically used for high-specification filtration in many laboratory applications. The fabrication process consists in the ion bombardment of membranes, commonly PET, at high energy and low fluencies and in a post-chemical etching of the damaged material along the ion track. This ion beam technique creates energetic particles that are nearly identical and have almost the same energy; consequently the tracks produced by each particle are almost identical. The etching process involves passing the tracked film through a number of chemical baths, creating a clean, well-controlled membrane with good precision in terms of pore size (Ferain & Legras, 1997, 2001a, Quinn *et al.*, 1997). This etching process determines the size of the pores, with typical pore sizes ranging from 20 nm to 14 μm. Although the shape of the pores is significantly better than the tortuous path membranes, the spatial distribution is inhomogeneous. As can

be seen in the TEMs shown in figure 1, there are undamaged areas in the membrane as well as regions where two or more etched tracks combine. These broad pores are propitious points for mechanical fracture and decrease the filtration selectivity in respect to the majority of smaller pores.

So far, the membranes with highest flux performance were introduced by the Dutch company Aquamarijn, using the well established semiconductor technology (van Rijn *et al.*, 1999). These membranes, called Microsieves, are fabricated using optical lithography and chemical etching of a silicon nitride thin film grown on a silicon substrate. After defining the membrane in the silicon nitride film, the silicon substrate is back etched (Girones *et al.*, 2005). The final membranes have pores with excellent pores size and spatial distribution (Figure 1). The drawback of the Microsieve technology is the difficult control of fouling and, mainly, the high cost of the substrates. Whereas 200 mm diameter silicon wafers cost some hundreds of dollars, few kilometers of fluorpolymers films can be obtained at similar expense. Additionally, although silicon nitride is chemically resistant, it is not as chemically inert as fluorpolymer materials, which decreases its applicability. Similarly to the TEMs, the fabrication process of Microsieves is relatively time consuming and expensive.

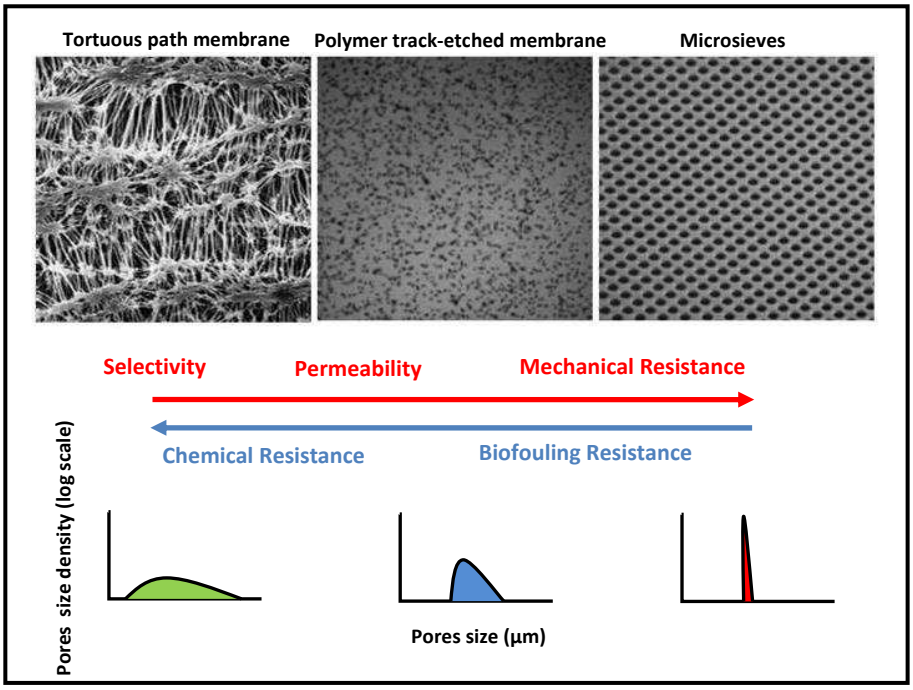

Fig. 1. Comparison of performance for different types of porous membranes. The direction of the arrows indicates improvement of the described properties. The bottom graphs schematically compare the pores size distribution for the membranes shown above.

3. Ion beam processing of PFA

Perfluoroalkoxyethylene is a fluoropolymer that has a carbon chain structure fully fluorinated in radicals and with a small amount of oxygen atoms. The chains are cross linked and are expressed by the molecular formula $[(CF_2CF_2)_nCF_2C(OR)F]_m$. PFA thin films have a broad range of applications in the packing and coating industry due to its thermal stability (melting point of approximately 304ºC), low adhesion, biological suitability and low frictional resistance (DuPont, 1996). PFA is solvent resistant to virtually all chemicals, which makes wet etch processing of these materials difficult or even impossible (Caplan *et al.*, 1997).

In this section, we evaluate the use of ion bombardment as an alternative tool for the processing of fluorpolymers, specifically Perfluoroalkoxyethylene irradiated with 5 MeV Au^+ ions. When ion beam irradiation is applied to process polymers, some parameters must be taken into consideration such as the surface modification, the polymer mobility and destruction, the charge-up effect in insulators, heat dissipation and recombination with molecules in the post bombardment environment. (Bachman *et al.*, 1988; Balik *et al.*, 2003; Evelyn *et al.*, 1997; Parada *et al.*, 2004, 2007a; Minamisawa *et al.*, 2007, 2007a).

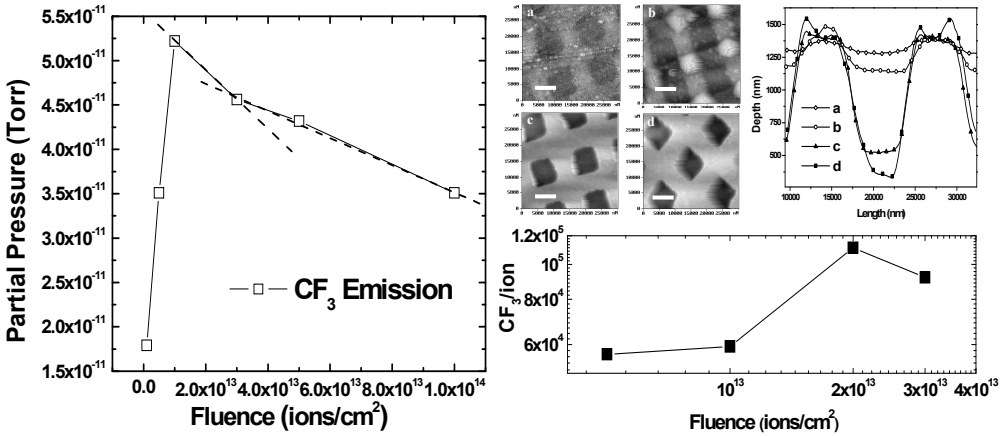

Fig. 2. Gas emission and mass loss of bombarded PFA thin films. The left plot shows the RGA profile of PFA films bombarded at different accumulated fluence. Atomic force microscopy images and the depth profiles (top-right) of the patterned films bombarded respectively with: a) 5×10^{12}, b) 1×10^{13}, c) 2×10^{13} and d) 3×10^{13} Au^+/cm^2. The scale in the AFM images represents 5 μm. The calculated physical etching yield for different implantation fluencies is shown in the bottom-right graph.

Data concerning mass loss of the ion bombarded PFA have been provided by two kinds of experiments: Measurment of the released gaseous species during bombardment and the the physical etching yield by surface analysis after irradiation. The PFA film thickness was 12.5 μm in all experiments.

In-situ Residual Gas Analyser (RGA) monitored a substantial emission of CF_3 molecules species from the PFA polymer film while bombarded at a maximum accumulated fluence of 1×10^{14} Au^+/cm^2 (Figure 2). The weak bonds between conjugated carbon when compared with F-C bonds and the relative higher mobility of the small radicals compared with the carbonic chains justify the higher emission of CF_3 gases during the ion beam modification. The idea is that CF_2 radicals are broken from the carbonic chains and recombined with adjacent fluorine atoms. For fluences up to 1×10^{13} Au^+/cm^2, the gas emission increases and after this value decreases due to the high level of fluorine loss and induced carbon crosslinking to form a more stable graphitelike material.

Figure 2 shows the atomic force microscopy AFM image of samples stenciled while bombarded at different accumulated fluences. The calculated physical etching yield extracted from the topographic AFM images of PFA films is about 9.0×10^4 CF_3 molecules emitted per incident ion. This value is more than 10^3 times higher than the sputtering yield simulated by TRIM06 software (Ziegler *et al.*, 1985). This deviation is attributed to thermal evaporation of the polymer. At low ion beam currents, low physical etching yield was observed, supporting the influence of thermal sublimation.

Figure 3a displays the Raman spectra of a thin PFA film and one bombarded at 1×10^{13} Au^+/cm^2 fluence, showing the presence of CF and CO bonds with peaks around 731.0 and 1381.1 cm^{-1}, respectively. At 1×10^{14} Au^+/cm^2 fluence the accumulated yield increased by a factor of ten for the same acquisition time while conserving the original bonds. This effect is attributed to enhanced fluorescence due to the influence of the implanted Au particles impurities on the PFA surface that formed nanometer sized metal clusters or surface grains. The PFA characteristic CF and CO bonds signals disappear in the sample bombarded at 1×10^{15} Au^+/cm^2 fluence, giving place to the D and G vibrational modes from amorphous carbon with peaks around 1329 and 1585 cm^{-1}, respectively. The D band is assigned to zone centers phonons of the E_{2g} symmetry and the G band to K-point phonons of the A_{1g} symmetry (Ferrari & Robertson, 1999).

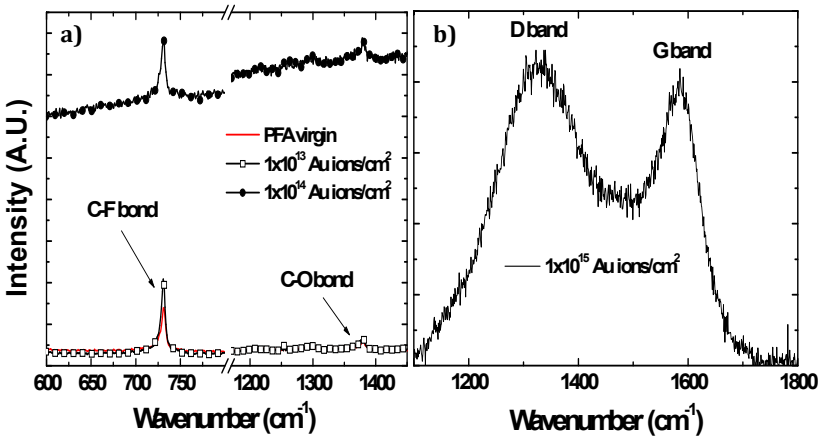

Fig. 3. Raman analysis of PFA thin films bombarded at different accumulated fluencies. At fluencies lower than 1×10^{14} Au^+/cm^2 (a), no significant change is observed in the PFA chemical bonds. At 1×10^{15} Au^+/cm^2 (b) accumulated fluence, the polymeric chains are modified to a graphite-like chemical structure due to substantial fluorine emission.

4. Probing pore formation

The fabrication of pores in freestanding PFA thin membranes by direct ion bombardment was controlled by a feedback system. The apparatus monitors the nanopore diameter when the ion beam impinges the polymer membrane defining a hole through which He gas is released and detected in an *in-situ* RGA (figure 4). PFA films were stenciled by a 2000 sq/inch mesh (5 × 5 μm^2 square shape openings) while bombarded by a 5 MeV Au^{+3} ion beam.

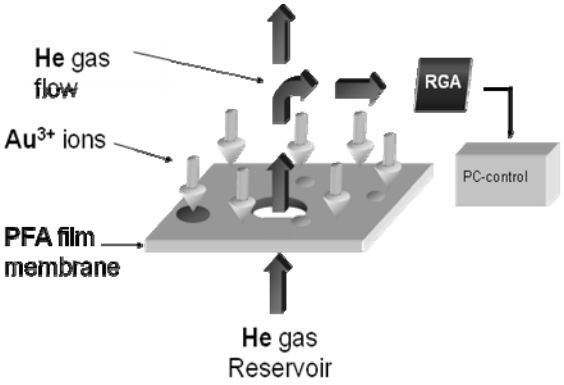

Fig. 4. Core idea of the feedback system built to monitor the pore formation. The pore formation in the PFA thin membrane, created by ion-induced physical etching, releases He gas from the reservoir, which is detected by the RGA and monitored in the PC control.

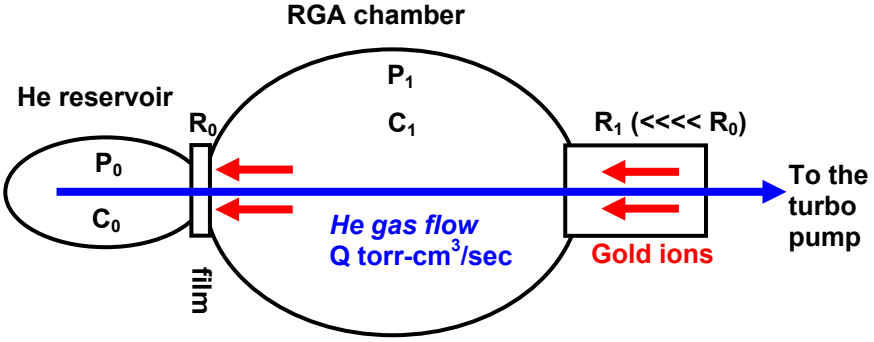

Fig. 5. Schematic of the experimental set-up for pore fabrication. The finite He gas supply contained in the reservoir has an initial pressure P_0 in the order of 10^3 Torr, while the RGA reads the He partial pressure P_1 of the order of 10^{-7} to 10^{-10} Torr. Helium partial pressure near the turbo pumps is in the order of 10^{-12} Torr. C_0 is the He reservoir volume (about 3 mm^3), C_1 is the RGA chamber volume (about 10^3 cm^3) and R_0 is the impedance (sec/cm^3) of the membrane that is many orders larger than the impedance of the 3 mm orifice R_1 to the beam line vacuum pumps. The red arrows symbolize the 5 MeV gold ion beam.

Figure 5 shows a schematic of the feedback system, where P and C denote, respectively, pressure and volume of the compartments and R the impedance of the gas channels. Specifically, the behavior of the system can be described as a gas flow through a channel with a difference of pressure, which defines the conductance $1/R$ as the rate flow per unity difference of pressure. Because of the light atomic mass, He diffusion through the PFA membrane is observed even before the pore formation. Therefore, the gas flow through the membrane has one dynamic before the opening of the pore ($t<t_0$) and another after the pore formation ($t>t_0$). The approximate solutions of the pressure behavior inside the RGA chamber (P_1) for $t<t_0$ and $t>t_0$ are given, respectively, by equations 1 and 2 (Dushman, 1962):

$$P_1 = P_0 \frac{R_1}{R_0}\left[1 - e^{-\frac{t}{R_1 C_1}}\right] e^{-\frac{t}{R_0 C_0}} \qquad t<t_0 \tag{1}$$

$$P_1 = P_0 e^{-\frac{t_0}{R_0 C_0}}\left[e^{-(t-t_0)\left(\frac{1}{R_p}+\frac{1}{R_0}\right)\frac{1}{C_0}}\right] R_1\left(\frac{1}{R_0}+\frac{1}{R_p}\right) \qquad t>t_0 \tag{2}$$

$$\tau_2 = R_{eff} C_0 \qquad 1/R_{eff} = 1/R_p + 1/R_0$$

When pores are formed, i.e., two or more gas conductances are connected in parallel, the total impedance is determined by the reciprocal of the sum of the inverse of R for each channel. The observance of the time constants before $\tau_0 = R_0 C_0$ and after $\tau_2 = R_{eff} C_0$ pore formation determines the conductance $1/R_p$ of the pores with the formula below equation 2. The value of the conductance $1/R_p$ enables the calculation of the pore dimensions.

Figure 6 displays a logarithm representation of the pressure in the RGA chamber $P_1(t)$, observed for two samples. The experimental results are fit using equations 1 and 2. The $1/e$ characteristic time constant $R_0 C_0$ is about 2.65 minutes for both samples. Using the value of the volume C_0 of 2.5 x 10^{-3} cm^3, we have an accurate determination of the gas diffusion impedance of the film R_0 = 7.9 × 10^4 sec/cm^3. A transient rise in pressure observed during pores formation is a "relaxation" effect, easily understood as the transition to a higher pressure in the RGA chamber volume. The observance of the transient rise signal is used as the initial time t_0 for triggering the feedback system, since it corresponds to the opening of pores. The ion beam is then blocked after a final time t_f, so the ion fluence accumulated during $\Delta t = t_f - t_0$ is used to control the final pores diameter. Notice that the ion beam current was optimized and kept constant during the system calibration. After Δt, the time constant $R_{eff} C_0$ is lowered in respect to $R_0 C_0$ as an indication of the additional conductance of the created pores. From figure 6, the time constants $R_{eff} C_0$ extracted for Δt_1 = 1 and Δt_2 = 1.5 minutes are, respectively, 1.88 minutes and 1.0 minutes. Considering that 1360 pores

were simultaneously fabricated, the average of conductance per pore calculated using the formula below equation 2, are $1/R_p(\Delta t_1)$ = 5.7 × 10^{-9} sec/cm^3 and $1/R_p(\Delta t_2)$ = 2.3 × 10^{-8} sec/cm^3.

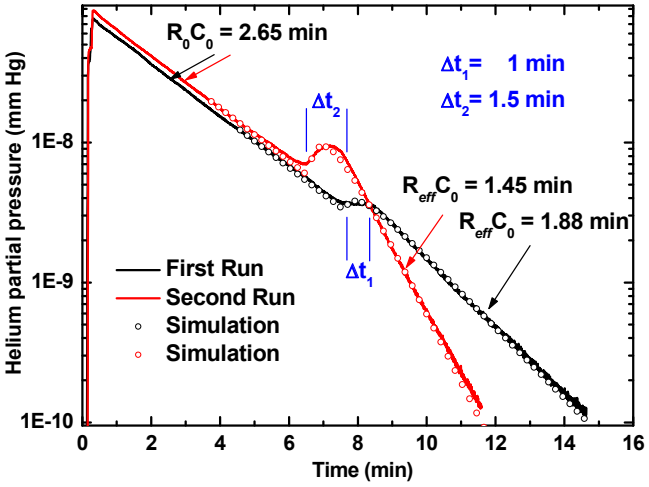

Fig. 6. RGA monitoring signal measured for two PFA samples bombarded during different times Δt. After blocking the ion beam, the time constant $R_{eff}C_0$ is lowered with respect to R_0C_0 as an indication of the additional conductance of the created pores. The off-set between t_0 in Δt_1 and Δt_2 is attributed to a small variation on the film thickness.

Considering that the mean free path of He in the experimental conditions is λ = 8.8 × 10^{-4} cm or 8800 nm, larger than the 50 nm to 2 µm pores produced by ion bombardment, the He gas flow through the pores is in the free molecular flow regime, where the atoms do not collide with each other while passing through a pore. The following equation gives a convenient numerical version of the conductance of a cylindrical tube with length L and radius a at 300 K temperature (Dushman):

$$1/R = 0.032\frac{a^3}{L} \quad \text{liters/sec} \tag{3}$$

Substituting the conductance per pore extracted from figure 6 in equation 3 for a 12.5 µm channel, pore diameters measured by the RGA are $D_{RGA}(\Delta t_1)$=260 nm and $D_{RGA}(\Delta t_2)$=415 nm. These results are higher than the ones measured by AFM images of $D_{AFM}(\Delta t_1)$≈100 nm and $D_{AFM}(\Delta t_2)$≈300 nm, which suggests that the effective channel lengths are smaller and that the conduits are not perfect cylindrical tubes.

5. PFA thin porous membranes

Optical microscopy inspection of the fabricated membranes reveals different dimensions of the pores in the bombarded and in the opposite face of the film. Whereas the pore sizes in the bombarded face is constant and equivalent to the stencil mask shape, the pore dimensions in the non-bombarded face can be controlled by tuning the accumulated ion fluence. Therefore, the membrane conduits have conical-like shapes and the pore size in the non-bombarded face defines the effective filtration area. This result confirms the variation in the pore diameters extracted from the RGA measurements.

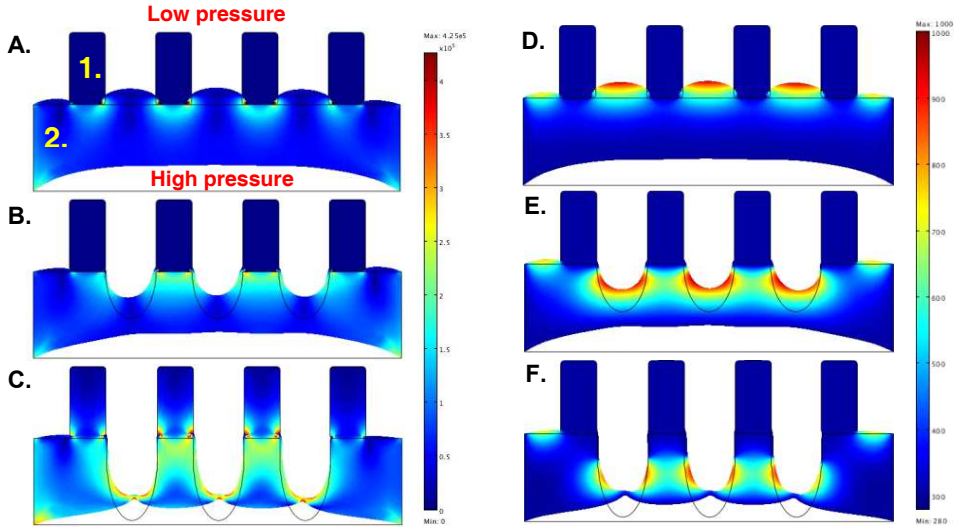

Fig. 7. Finite element simulations of strain and temperature superposed by deformation of the film during bombardment of the stencil masked PFA films. The black line represents the shape of the film without pressure-induced deformation. The PFA film is indicated by 1 while the metal mask is indicated by 2. The pressure across the film leads to deformation of the soft film, constrained by the metal mask. The strain (A, B and C) in the unmasked areas is lower than in the masked ones, which creates low density regions that allow higher ion penetration. Simultaneously, the metal mask acts as a heat sink for the power delivered by the ion beam, which focus the temperature in the center of the unmasked areas (D, E and F).

The pore shape and the high physical etching yield is explained in terms of thermal and strain effects that act in the polymer during irradiation as shown in the COMSOL simulations in figure 7. The strain acting in the unmasked areas decreases the density of polymer chains in the center of these regions, allowing higher penetration of gold ions, and consequently concentrated bond scissoring (figure 7A and B). In the instant of the pore formation, the strain effect is directly responsible for the pores opening (figure 7C). Simultaneously, the metal mask acts as a heat sink for the power delivered by the ion beam, leading to high temperature concentration (up to 1000°C) in the center of the unmasked areas of the polymer film (figure 7D and E). Although a complete phase diagram for PFA is

not readily available in the literature, assuming the PFA melting point of around 310°C, sublimation at 1000°C may be a possible explanation for the high physical etching yield during bombardment. Combined, both effects lead to a concentration of physical etching in the center of the unmasked areas, and consequently, to the conical-like shape formation of the conduits.

Figure 8 shows the Raman scattering spectra extracted inside and in a non-bombarded adjacent area of a pore fabricated at 1 × 10^{13} Au^+/cm^2 fluence. The C-F and C-O bonds inside the pore are conserved when compared with the masked area. This is an evidence of the fluorpolymer property to decompose under ion bombardment leaving relatively undamaged material.

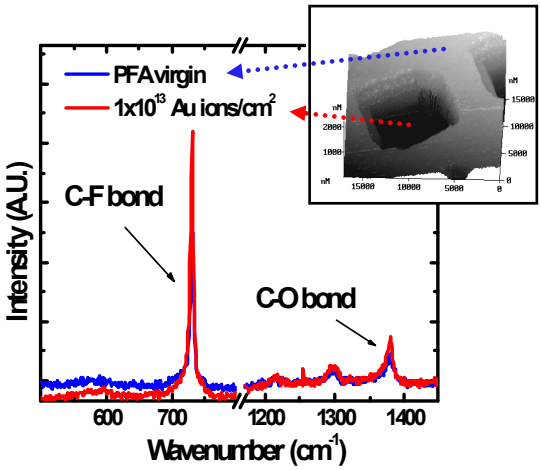

Fig. 8. Damage analysis in one processed pore evaluated by Raman spectroscopy. The graph compares the Raman spectra measured inside one pore and in an adjacent masked area (inset AFM image). The chemical structure of the pores is unchanged after 1 × 10^{14} Au^+/cm^2 implantation, consequently, keeping the polymer material properties.

At 1 × 10^{14} Au^+/cm^2, circular micropores with ~2 µm diameter and uniform distribution in space were fabricated in the non-bombarded face of the PFA thin film membrane as shown in the optical microscopy image on figure 9. The impression that some pores are closed is attributed to focus artifact, however, the inset AFM image confirms that all the pores are effectively opened. Distances between adjacent pores have an average of approximately 12 µm, which matches with the center of the collimation squares in the stencil mask.

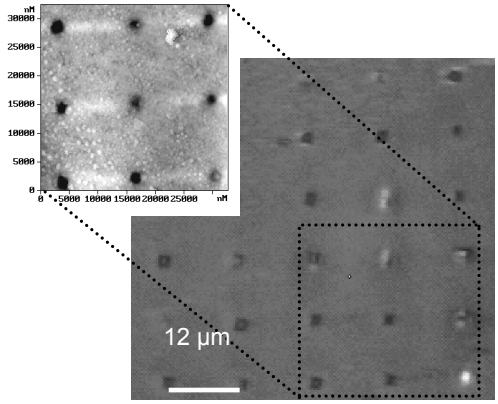

Fig. 9. Optical microscopy and AFM images of a PFA microporous membrane. Although the optical microscopy images gives the impression that some pores are closed due to artifacts of measurement, the AFM topography image (inset) confirms that all pores are opened.

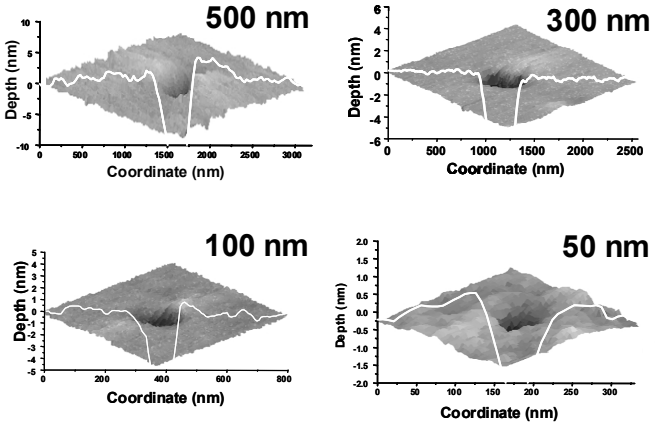

Fig. 10. Atomic force microscopy images superposed by topography profiles of nanopores with diameters ranging from 50 to 500 nm.

The PFA porous membranes fabricated by direct ion-induced physical etching have better pore size and spatial distribution compared to the tortuous path and polymer track-etched membranes, while maintaining the fluorpolymer properties. Simultaneously, the PFA porous membrane filtration capacity is almost comparable to the high-flux microsieve silicon nitride membranes. Figure 10 shows the AFM images superposed on the topography profiles of nanopores with 50, 100, 300 and 500 nm diameters fabricated at different accumulated fluence. Having pores at scales smaller than 500 nm, the PFA porous membranes are strong, chemically resistant membranes for air monitoring and sampling in aggressive environments. At this scale, bacteria or other microorganisms can be filtered in water or air treatment.

6. Conclusions

In this chapter we firstly assessed the current stage of development of porous thin film membranes for filtration applications. As discussed in the introduction, porous membrane performance requires high permeability, high selectivity, enhanced resistance to biofouling, and resistance against solvents, high- and low-pH environments, and oxidizers. Additionally, the cost-effectiveness of this technology is a major concern for financially disadvantaged societies with scarce water resources. ***Innovative processes for fabrication of porous membranes as well as the development of new polymer precursors is the key solution***.

Finally, we report our recent development in the fabrication of PFA fluorpolymer porous thin film membranes by ion-induced physical etching using a stencil mask technique. PFA fluorpolymers are candidates for advanced filtration membranes for being chemically inert, potentially resistant to biofouling because of its lowest adhesion coefficient known. We show that Au+ ion bombardment at specific conditions is able to induce a high level of physical etching through mechanical sputtering, enhanced by thermal sublimation of the PFA film. In our process, porous membranes with homogeneously distributed pores down to 50 nm diameter were fabricated. Chemical structure analysis demonstrate that the post-processed pore channels are relatively undamaged, consequently, maintaining their chemical resistant properties. Lastly, we presented the development of a feedback ion beam controlled system able monitor in real time the pore formation, by monitoring the gas flow through the bombarded films.

PFA porous membranes potentially ***offer a combination of the high performance of the microsieve membranes and the cost-effectiveness and resistant material performance of fluorpolymer membranes***. At the present stage, our PFA porous thin film membranes are a realistic alternative to substitute the low-flux performance fluorpolymer tortuous path membranes. Further research must be focused in different ion beam parameters, possibly in high current ion beam bombardment, and in the application of the process in similar fluorpolymers materials such as ETFE and FEP.

7. References

Bachman B. J., & Vasile M. J. (1988). *Proceedings of the IEEE 38th Electronics Components Conference*. Los Angeles, CA.

Balik, C. M., Said, M. A., & Carlson, J. D. (2003). High-energy ion implantation of polymers: Poly(ethylene terephthalate). *Journal of Polymer Science, Part B: Polymer Physics*, 25(4), 817-827.

Caplan, M. R., Chiang, C. Y., Lloyd, D. R., & Yen, L. Y. (1997). Formation of microporous Teflon® PFA membranes via thermally induced phase separation. *Journal of membrane science*, 130, 219-237.

Dushman, S. (1962). *Scientific Foundations of Vacuum Technique*. New York, NY: John Wiley & Sons.

DuPont. (1996). PFA Films bulletin: http://www2.dupont.com/Teflon_Industrial/en_US/assets/downloads/h04321.pdf

Evelyn, A. L., Ila, D., Zimmerman, R. L., Bhat, K., Poker, D. B., & Hensley, D. K. (1997). Resolving the electronic and nuclear effects of MeV ions in polymers. *Nuclear Instruments and Meth*ods B, 127/128, 694.

Ferrari, A. C., & Robertson, J. (1999). Interpretation of Raman spectra of disordered and amorphous carbon. *Physics Review B*, 61, 14095-14107.

Ferain, E., & Legras, R. (1997). Characterization of nanoporous particle track etched membrane. *Nuclear Intruments and Methods in Physics Research Section B*, 131, 97-102.

Ferain, E., & Legras, R. (2001). Characterization of nanoporous particle track etched membrane. *Nuclear Intruments and Methods in Physics Research Section B*, 174, 116-122.

Fologea, D., Gershow, M., Ledden, B., McNabb, D. S., Golovchenko, J. A., & Li, J. (2005). Detecting single stranded DNA with a solid state nanopore. *Nanoletters,* 5, 1905-1909.

Girones, M., Lammertink, R. G. H., & Wessling M. (2005). Protein aggregate deposition and fouling reduction strategies with high-flux silicon nitride microsieves. *Engineering with membranes: Medical and Biological Applications*, 273(1-2), 68-76.

Henriquez, R. R., Ito, T., Sun, L., & Crooks, R. M. (2004). The resurgence of Coulter counting for analyzing nanoscale objects. *Analyst*, 129, 478-482.

Li, J., Gershow, M., Stein, D., Brandin, E., & Golovchenko, J. A. (2003). DNA molecules and configurations in a solid-state nanopore microscope. *Nature Materials*, 2, 611–615.

Li, J., Stein, D., McMullan, C., Branton, D., Aziz, M. J., & Golovchenko, J. A. (2001). Ion-beam sculpting at nanometer length scales. *Nature*, 412, 166-169.

Minamisawa, R. A., Almeida, A., Abidzina, V., Parada, M. A., Muntele, I., & Ila, D. (2007). Effects of low and high energy ion bombardment on ETFE polymer. *Nuclear Instruments and Methods in Physics Research B*, 257, 568-571.

Minamisawa, R. A., Almeida, A., Budak, S., Abidzina, V., & Ila, D. (2007). Surface damage studies of ETFE polymer bombarded with low energy Si ions (<100 keV). *Nuclear Instruments and Methods in Physics Research B,* 261, 1159-1161.

Mochel, M. E., Eades, J. A., Metzger, M., Meyer, J. I., & Mochel, J. M. (1984). Electron beam cutting in amorphous alumina sheets. *Applied Physics Letters*, 44(5), 502-505.

Mutoh, Y. (1987). Porous fluorine resin membrane and process for preparing the same. U.S. Pat. Nº 4,702,836. Fujisawa, JP.

Parada, M. A., Minamisawa, R. A., Almeida, A., Muntele, C., Zimmerman, R. L., Muntele, I., & Ila, D. (2004). Fluoropolymer studies for radiation dosimetry. *Brazilian Journal of Physics*, 34, 948-950.

Parada, M. A., Minamisawa, R. A., Moreira, M. V., Almeida, A., Muntele, I., & Ila, D. (2007). Damage effects of gamma and X-rays in polymer film electrets. *Surface and Coatings Technology*, 201, 8246-8249.

Quinn, J., Anderson, J. L., Ho, W. S., & Petzny, W. J. (1972). Model pores of molecular dimension: the preparation and characterization of track-etched membranes. *Biophysical Journal*, 12 (8), 990-1007.

Rogers, R. (1998). Membrane Materials. *Chemical Engineering News*, 76(34), 38-39.

Schenkel, T., Radimilovic, V., Stach, E. A., Park, S. J., & Persaud, A. (2003). Formation of a few nanometer wide holes in membranes with a dual beam focused ion beam system. *Journal of Vacuum Technology B,* 21(6), 2720-2723.

Vainrot, N., Eisen, M. S., & Semiat, R. (2008). Membranes in Desalination and Water Treatment. *MRS Bulletin*, 33, 16-20.

Van Rijn, C. J. M., Nijdam, W., Kuiper, S., Veldhuis, G. J., van Wolferen, H., & Elwenspoek, M. (1999). Microsieves made with laser interference lithography for micro-filtration applications. *Journal of Micromechanical Microengineering*, 9, 170-172.

Ziegler, J. F., Biersack, J. P., & Littmark, U. (1985). *The Stopping and Range of Ions in Solids*, New York, NY: Pergamon Press.

Polymer Thin Films

Edited by Abbass A Hashim

ISBN 978-953-307-059-9
Hard cover, 324 pages
Publisher InTech
Published online 01, April, 2010
Published in print edition April, 2010

This book provides a timely overview of a current state of knowledge of the use of polymer thin film for important technological applications. Polymer thin film book covers the scientific principles and technologies that are necessary to implement the use of polymer electronic device. A wide-ranging and definitive coverage of this emerging field is provided for both academic and practicing scientists. The book is intended to enable readers with a specific background, e.g. polymer nanotechnology, to become acquainted with other specialist aspects of this multidisciplinary field. Part A of the book covers the fundamental of the key aspect related to the development and improvement of polymer thin film technology and part B covers more advanced aspects of the technology are dealt with nano-polymer layer which provide an up-to-date survey of current research directions in the area of polymer thin film and its application skills.

INTECH
open science | open minds

InTech Europe
University Campus STeP Ri
Slavka Krautzeka 83/A
51000 Rijeka, Croatia
Phone: +385 (51) 770 447
Fax: +385 (51) 686 166
www.intechopen.com

InTech China
Unit 405, Office Block, Hotel Equatorial Shanghai
No.65, Yan An Road (West), Shanghai, 200040, China
中国上海市延安西路65号上海国际贵都大饭店办公楼405单元
Phone: +86-21-62489820
Fax: +86-21-62489821